Numerical Studies of Moment-Rotation Behavior in Steel and Composite Steel-Concrete Bridge Girders

DONALD W. WHITE AND AMIT DUTTA

Presented in this paper are the results from several finite element studies of the inelastic moment-rotation behavior of continuous-span noncompact bridge girders at interior-pier locations. Specifically, four component tests, which have been conducted experimentally in previous research supported by the American Iron and Steel Institute, are performed numerically in the present work. Three of the test specimens are all-steel girders and one is a composite design. All of the specimens were designed with ultracompact flanges and with closely spaced transverse stiffeners in the peak negative moment region. The web slendernesses vary from being nearly compact to the extreme range allowed for design of transversely stiffened girders. The analysis results for these tests are compared with the experimental responses, and aspects of the behavior elucidated by the finite element predictions are discussed. These studies confirm that continuous-span noncompact bridge girders can exhibit a significant and reliable capacity for inelastic rotation at interior supports.

During the past 9 years, the American Iron and Steel Institute (AISI) has been sponsoring a steel bridge research program aimed in part at extending alternate load factor design (ALFD) concepts (*1*) to noncompact plate-girder sections. This work has culminated recently in the development of a unified analysis procedure for design at the American Association of State Highway and Transportation Officials (AASHTO) service load, overload, and maximum load levels (*2*). The unified analysis approach can account for plastification at any number of locations throughout the spans of a continuous girder, and involves the direct use of moment-rotation curves that characterize the response at zero-length "plastic hinging" locations.

Inelastic moment-rotation curves have been generated experimentally for a range of transversely stiffened noncompact girder sections, both at interior-pier locations (*3–5*) as well as at maximum positive-moment locations (*6*). However, these tests represent only a sparse sampling throughout the full range of design characteristics possible in actual bridge girders. Consequently, additional studies are needed to support, and perhaps refine, the characteristic moment-rotation curves used for design analysis.

Research directed at the use of finite element methods for elucidation of the factors that influence the interior pier moment-rotation characteristics of noncompact steel bridge girders is reported in this paper. A major focus of the report is on the correlation of analysis predictions with experimental results from component tests conducted by Schilling and Morcos on three noncomposite steel girders (*4*), and with the results from a recent composite girder conducted by Tansil (*5*).

School of Civil Engineering, Purdue University, West Lafayette, Ind. 47907.

DESCRIPTION OF TEST SPECIMENS

The geometric parameters of the all-steel specimens are illustrated in Figure 1, and the composite specimen is shown in Figure 2. These specimens were designed to study the behavior within the negative moment region of continuous span bridge girders. As shown in the figures, all of the specimens are loaded at their midlength (simulating the conditions at an interior pier), and they are simply supported at their ends (simulating the location of an inflection point in the prototype girder). The all-steel girders were loaded in an inverted position to simplify testing.

All of the girders were designed with ASTM A572 Grade 50 steel, ultra-compact flanges [i.e., the flanges were proportioned to satisfy the conventional requirements for plastic design from Part 2 of the 1978 AISC Specification (*7*)], lateral bracing at intervals satisfying the lateral support requirements of the ALFD Guide Specifications (*1*), noncompact webs, and closely spaced one-sided transverse stiffeners within the peak moment region. Additional one-sided transverse stiffeners were provided between the peak moment region and the end of the beams to resist shear buckling. The spacing of these stiffeners was selected so that the maximum shear would be approximately $0.6V_u$, where V_u is the ultimate shear capacity as limited by tension-field action (*8*). The web slenderness of the all-steel girders ranged from a value that is nearly compact for Specimen *S* to a value that is at the upper limit for classification as noncompact for Specimen *D*. The composite girder web was similar in slenderness to that of Specimen *D*.

The span lengths of the all-steel specimens were selected to produce a high level of shear stress in the web. The shear force V was approximately equal to $0.55V_p$ in each of these tests, where V_p is the plastic shear capacity of the web (*8*). However, in exploratory ALFD designs of noncompact girders (*9*), the highest V/V_p in the maximum load check was 0.33. The composite girder test specimen was designed to reach its peak capacity approximately at this value of shear force.

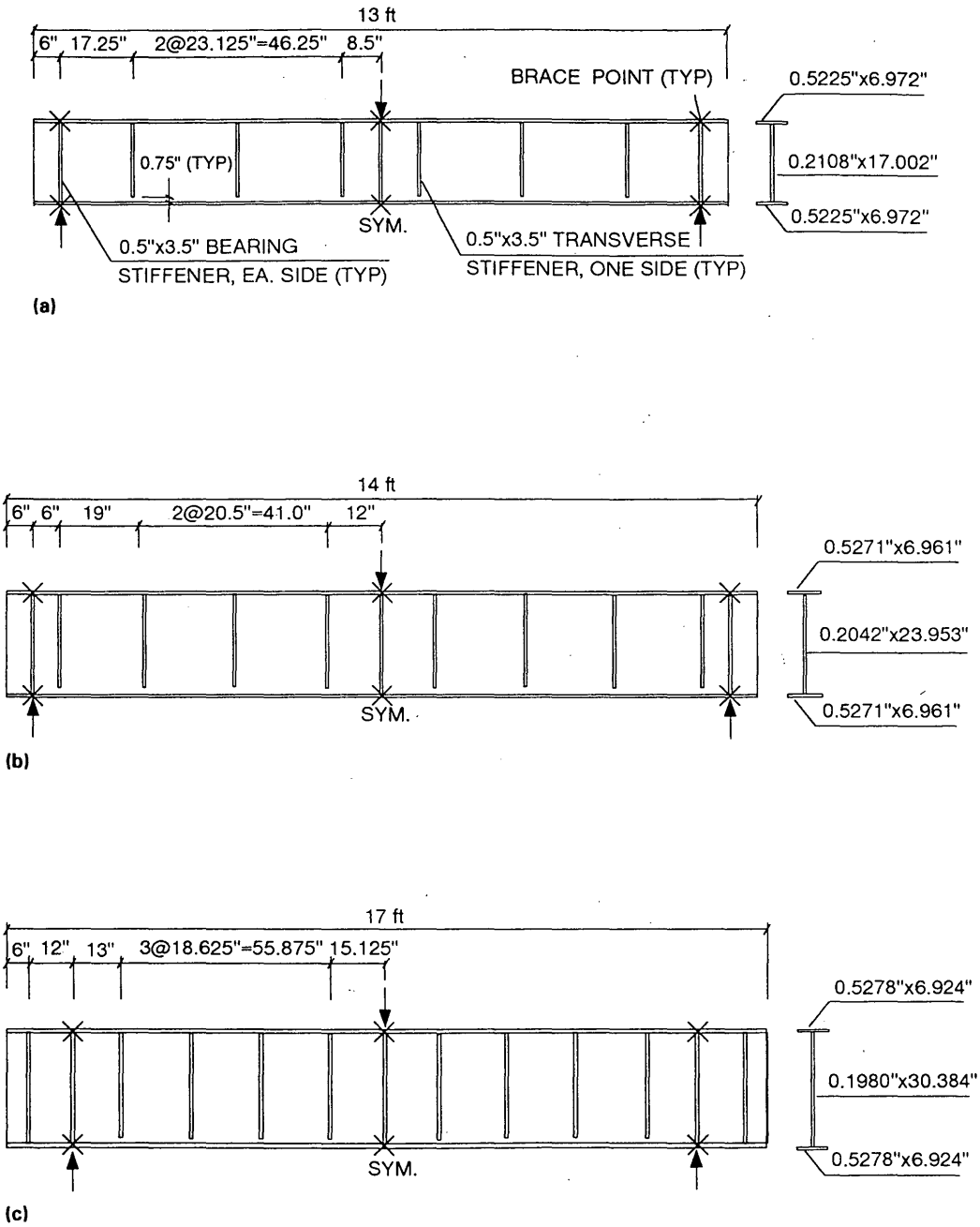

FIGURE 1 All-steel test specimens (*4*): (a) Specimen *S*, (b) Specimen *M*, and (c) Specimen *D*.

FUNDAMENTAL BEHAVIOR AND ANALYSIS APPROACH

The physical and behavioral aspects that can influence the inelastic moment-rotation behavior of noncompact steel plate girders include

1. Initial imperfections such as out-of-flatness, bowing, or twisting of the web and flange plates, as well as the overall initial sweep and twisting of the girder cross section along the span length;
2. Residual stresses caused by fabrication and welding;
3. Spread of plasticity, including strain-hardening and multidimensional plasticity effects;
4. Cross-section distortion; and
5. Interaction of various local and overall modes of instability; that is, local flexural and shear buckling of the web panels, local buckling of the flange plates, and lateral buckling of the girder between brace points.

A shell finite element approach is chosen in this work as being both necessary and sufficient for modeling of these aspects. Detailed aspects of the finite element model are described by White and Dutta (*10*). An incremental-iterative

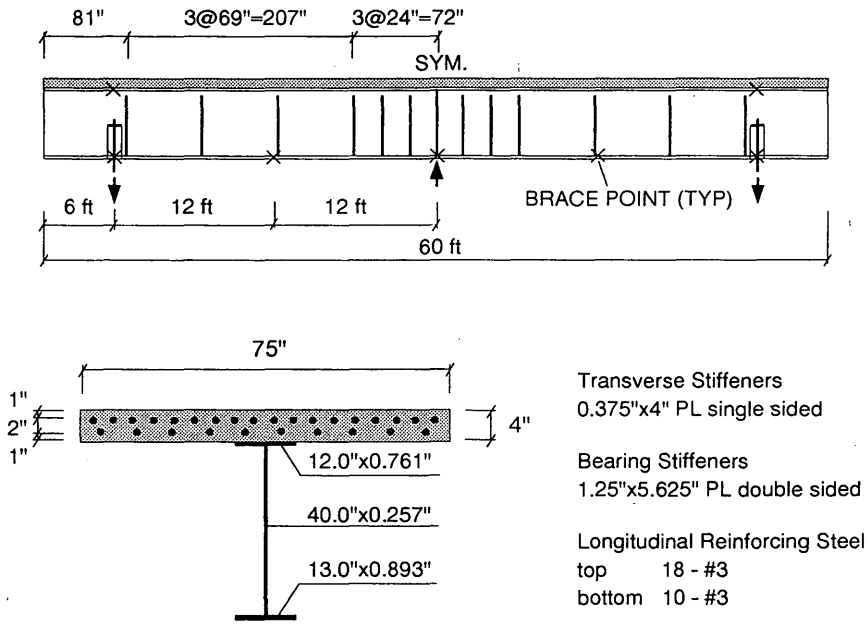

FIGURE 2 Composite test specimen (*5*).

analysis approach is employed in all the studies to capture the combined geometric and material nonlinear effects on the pre- and post-peak response of the test specimens.

REPRESENTATION OF PHYSICAL ATTRIBUTES FOR ANALYSIS

General Stress-Strain Characteristics

A single-surface plasticity model based on incrementally linear flow theory is employed for representation of the material response. The initial yield condition is represented by the von Mises yield function. Kinematic hardening of the yield surface is assumed, producing the trilinear effective stress-strain response shown in Figure 3. The yield stress F_y is taken as the average of the values measured in coupon tests of the flange and web steel. For the composite girder, the strain at incipient strain-hardening ε_{st} is also taken as the average of the values obtained from coupon tests. The other stress-strain parameters are typical values for A572-Grade 50 steel reported in the general literature. The stiffnesses within the yield plateau are typical of values used in successful correlations with experimental tests conducted by other investigators (*11*)

Residual Stresses

Residual stresses have not been reported for the test specimens, and indeed they are not easily obtained. Furthermore, it is expected that the residual stresses in actual welded bridge girders are highly variable and depend on very specific details of the fabrication and welding processes. Nevertheless, yielding is evident at very low load levels in the experimental tests (*4,5*). This confirms the expectation that the residual stresses at weld locations are essentially equal to the yield stress of the material in tension. Of course, smaller self-equilibrating compressive residual stresses must exist in the regions of the girders removed from the welds. For the analyses performed in this work, representative residual stress patterns of this nature are assumed in the longitudinal direction of the girders. The specific assumed patterns are illustrated in Figure 4.

In Specimen *S*, the maximum compressive residual stress in the web was taken as $-0.25F_y$. This value is typical for welded beam sections (*12*). However, for the other plate-girder sections with more slender webs, this value is greater than the elastic critical stress associated with uniform

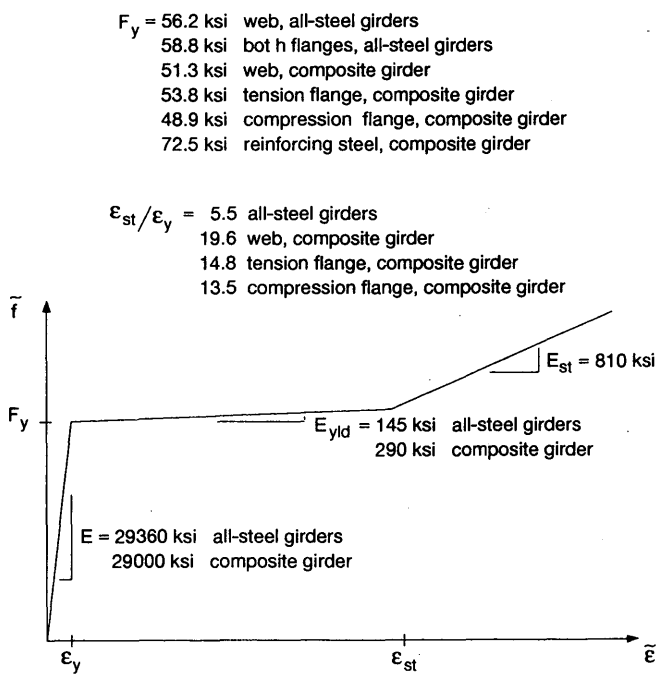

FIGURE 3 Effective stress-strain curves for analysis.

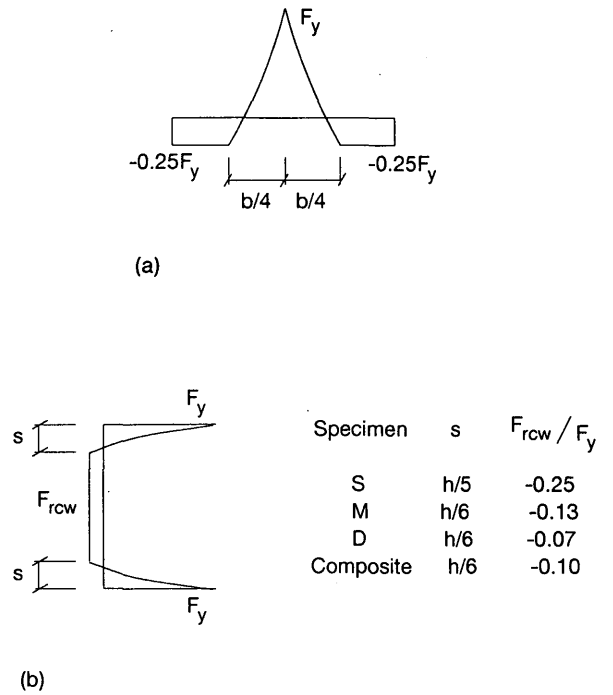

FIGURE 4 Assumed residual stress patterns: (a) flange residual stresses, self-equilibrating, all girders, and (b) web residual stresses, self equilibrating.

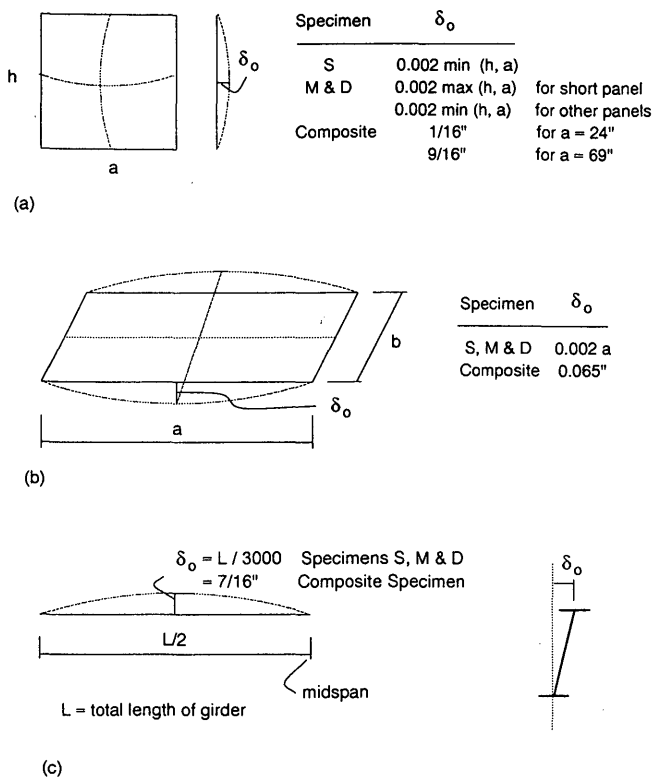

FIGURE 5 Initial imperfections: (a) initial out-of-flatness in each panel of web, (b) initial out-of-flatness in each panel of flange (compression flange only) and (c) overall sweep of compression flange.

compression of the web panels. Therefore, the compressive residual stresses in the other webs have been specified at approximately the same fraction of the elastic critical stress as that assumed for Specimen *S*. A parabolic distribution is specified for the transition between the peak tensile and compressive residual stresses in the girder cross sections, the parameters of this distribution being determined so that the residual stresses in the web and in the flanges are self-equilibrating.

Initial Imperfections

The specified initial geometric imperfections are illustrated in Figure 5. These imperfections match approximately the maximum out-of-flatness of the web panels reported in all the experimental investigations, and the maximum out-of-straightness caused by a lateral sweep of the compression flange reported for the composite girder. Furthermore, an initial out-of-flatness of the compression flange is assumed in all the analyses [see Figure 5(b)], and a sweep of the compression flange is assumed in the all-steel girder studies. A sinusoidal pattern is assumed for the imperfections in each panel of the girders, and the imperfections are specified in alternating directions from panel to panel along the girder length. The twisting of the compression flange in each panel is assumed to be in the same direction as the rotation at the web-flange junctions because of the web imperfections.

Modeling of Composite Concrete Deck

Experimental studies have shown that if the deck is not post-tensioned, there is essentially no assistance from the concrete in resisting the load at large plastic rotations (*5*,*13*). That is, the ultimate load behavior of the girder in the negative moment region is essentially that associated with a conventional cracked section analysis. Furthermore, recent work (Carskaddan, unpublished data) has elucidated the fact that concrete cracking contributes little to the inelastic rotation at interior-pier sections of continuous members. That is, after cracking has occurred, the state of the girder is essentially the same as that obtained for the steel girder plus reinforcing steel as if the concrete had never participated in resisting the load. Also, it is evident that significant concrete cracking can occur because of shrinkage, resulting in cracked section behavior even at small load levels (*5*). For these reasons, as well as the extreme complexity of the concrete behavior within the deck, the composite deck is assumed to be cracked before the start of the analysis in the present study.

Other Aspects of Analysis Models

All the test specimens are modeled on the basis of the assumption of symmetry about a vertical axis through the web at the midspan location. However, the actual behavior in experimental tests sometimes involves severe inelastic local and overall buckling on one side of the midspan, and elastic unloading on the opposite side of the load point. The symmetry assumption is conservative because any restraint provided by an elastically unloading half span is neglected.

In the testing of the composite specimen, the loading was applied to simulate unshored construction. For the analysis

of this test, the simulated dead load is applied to the steel girder alone, and all the additional loading is applied to the cracked composite section. The dead load level corresponds to a moment of 0.452 of the plastic moment M_p at the midspan of the girder.

RESULTS FOR SPECIMEN *S* (SHALLOW DEPTH WEB)

In Figure 6, the normalized moment at the midspan of the test specimen M/M_p is plotted versus the normalized plastic deflection of the girder at the load point, $2\Delta_p/L$, where L is the length of the halfspan of the girder. The analysis results are shown by the solid curve, whereas the experimental test results are plotted as a dashed line. The experimental test points are highlighted by the open boxes. The plastic deflection Δ_p is computed by subtracting the elastic component from the total deflection at the midspan of the specimen for each load level. The normalized value of this deflection $2\Delta_p/L$ gives the inelastic rotation that would be required within a "plastic hinge" at the midspan of the specimen if all plastic deformations are assumed to be concentrated within this zero-length hinge and plastic shear deformations are neglected. The value $2\Delta_p/L$ correlates well with the actual inelastic rotation measured in the test, which is indicated by the dotted curve in the figure. Therefore, it appears that the idealization of the inelastic moment-rotation curves as the behavior at a zero-length hinge is adequate. However, the normalized plastic deflection is slightly smaller than the actual inelastic rotation in the extreme post-peak region of the response. This is because significant local buckling and plastic deformation occurs in the second panel from midspan within the unloading branch of this test. Similar results are obtained for the other tests considered in this paper.

Snapshots of the magnified deflected shape of the girder are shown at the peak-load point and immediately subsequent to this point in Figures 7(a) and 7(b). These photographs are of the halfspan of the girder to the left of the load point only. Also, the bearing stiffeners at the end of the girder and at midspan are not shown. The transverse stiffeners are shaded.

The significant aspects of the behavior in this test, and the corresponding finite element predictions, may be summarized as follows:

1. The plots in Figure 6 indicate that the finite element results are somewhat stiffer than the experimental results in the range of loading before reaching the plastic moment M_p. It is believed that this discrepancy may be largely the result of transverse residual stresses in the specimen caused by welding of the stiffeners. This is based on observations of early transverse yielding at the stiffener locations in the composite girder of Figure 2 (*5*). Only longitudinal residual stresses were considered in the finite element studies.
2. The maximum moment obtained in the physical test of this specimen was 11 percent higher than the plastic moment capacity of the section. This strength is matched by the finite element predictions.
3. The normalized deflection at the peak load point is approximately the same in the experiment and the analysis.
4. The slopes of the unloading curves from the experiment and the analysis are essentially the same. The primary difference in the unloading curves is that the analysis model unloads abruptly over a short portion of the curve immediately after reaching the peak load.
5. The mode of failure predicted by the analysis is the same as that obtained in the experimental test. The deflected shape shown in Figure 7(a) illustrates that initially the web starts to bow under flexural compressive stresses. These web deformations do not occur abruptly, but instead increase gradually. As shown in the figure, the compression flange starts to rotate slightly about a longitudinal axis within the first panel and offers some restraint to the deformations in the web.
6. The distortion of the girder cross section at the peak-load capacity is essentially unnoticeable to the naked eye [the deformities shown in Fig. 7(a) are magnified five times].

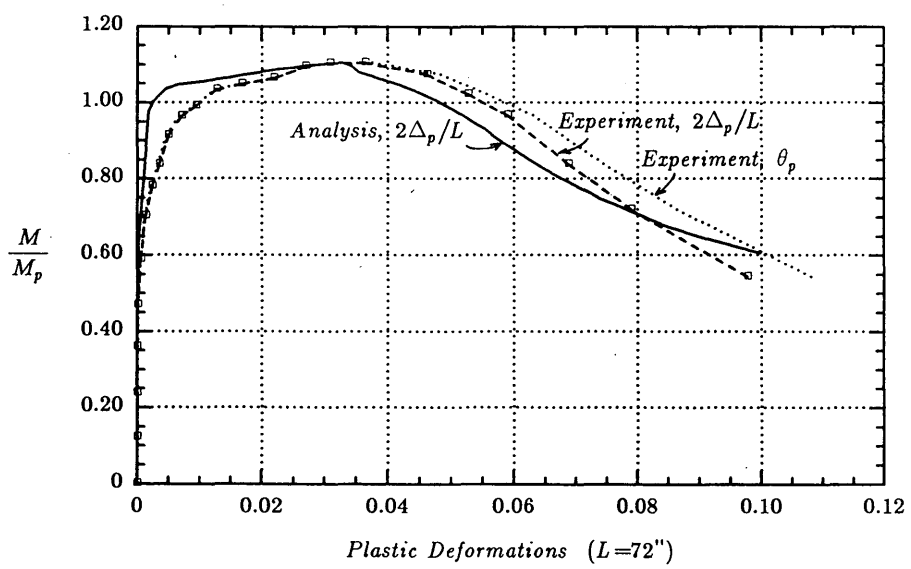

FIGURE 6 Normalized moment versus plastic deformations: Specimen *S*.

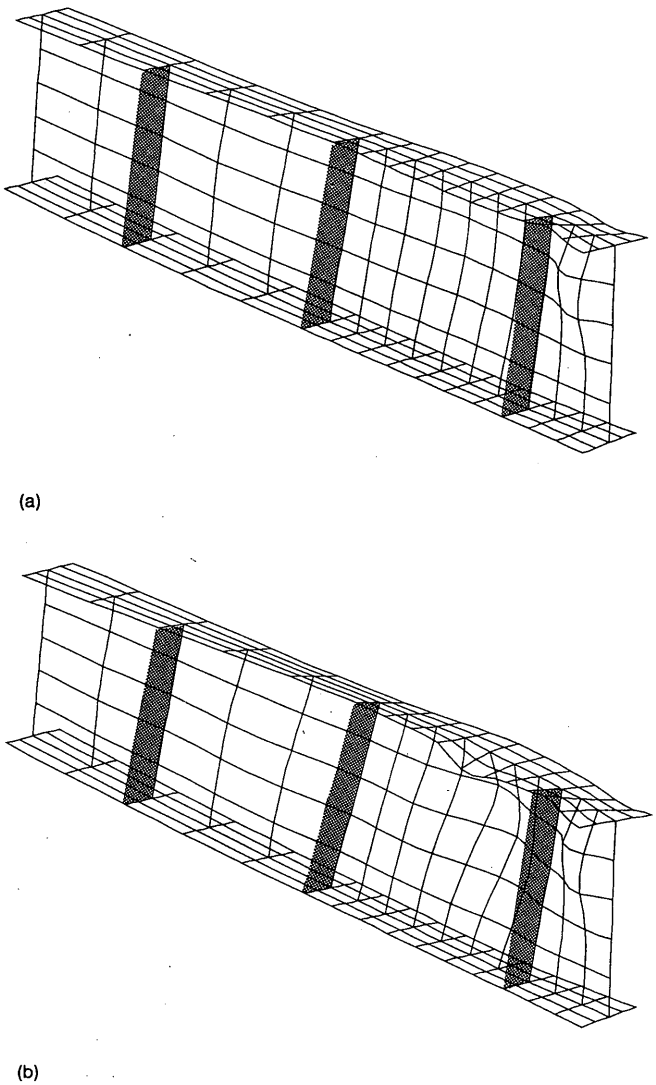

FIGURE 7 Deformed meshes during progress of the analysis: Specimen *S*: (a) at peak load capacity: $M/M_p = 1.105$, normalized plastic deflection $2\Delta_p/L = 0.0320$ ($L = 72$ in.), magnification of 5 times; and (b) immediately after unloading: $M/M_p = 1.045$, normalized plastic deflection $2\Delta p/L = 0.0432$ ($L = 72$ in.), magnification of 5 times.

7. When the peak load is reached, the mode of deformation of the girder changes suddenly and dramatically [compare Figs. 7(a) and 7(b)]. The second web panel from the midspan appears to buckle at this stage, and the primary deformations shift from the short panel adjacent to midspan to this longer panel.

8. The deformations in the second panel from the midspan continue to grow as the girder is deformed through the post-collapse region of the response. Three views of the girder at the end of the analysis are shown in Figure 8. This deflected shape is essentially the same as that of the most severely deformed half span of the experimentally tested girder (*4*). It is important to note that the final failure of the girder involves significant interaction between local web, local flange, and lateral-torsional buckling modes.

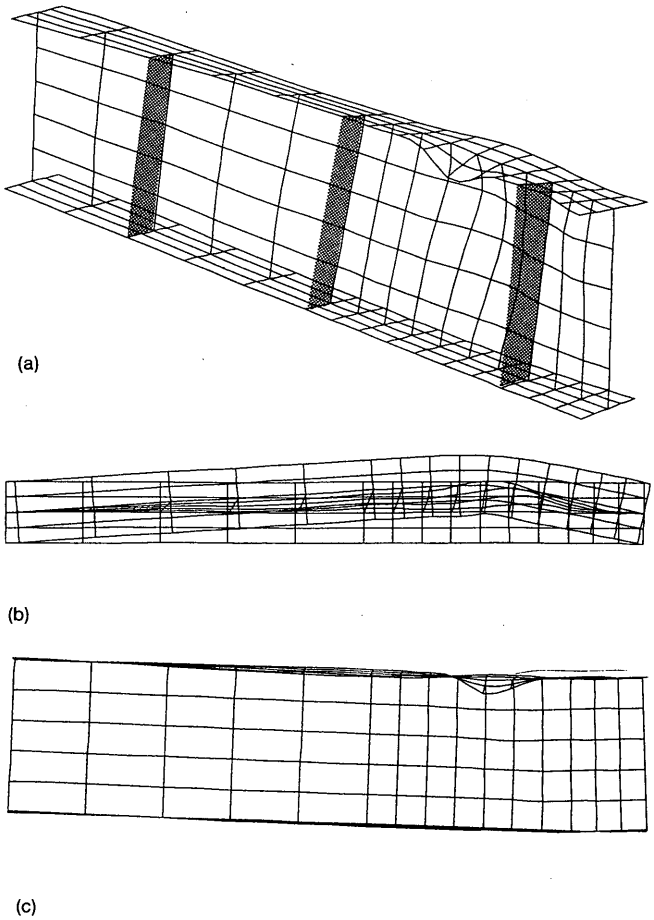

FIGURE 8 Deformed mesh at end of analysis, Specimen *S*, $M/M_p = 0.570$, normalized plastic deflection $2\Delta_p/L = 0.100$ ($L = 72$ in.), no magnification: (a) perspective view, (b) top view, and (c) side view.

RESULTS FOR SPECIMENS *M* AND *D* (MEDIUM DEPTH AND DEEP WEBS)

The results for Specimens *M* and *D* are presented in Figure 9. The behavior predicted from these studies is similar and therefore these tests will be discussed jointly. The following observations can be made from these analyses:

1. As in the analysis of Specimen *S*, the numerical results are initially too stiff. Possible reasons for this behavior have been outlined in the previous section. However, the peak load predictions for these girders are quite good. For Specimen *M*, the finite element analysis predicts a peak moment equal to the plastic moment M_p and in the experiment a peak moment of $1.02M_p$ was observed. The corresponding values for Specimen *D* are $0.93M_p$ and $0.90M_p$.

2. The deflection at the peak load capacity of these beams is not predicted as well as in the analysis of Specimen *S*. This appears to be primarily because of the initial over-stiff characteristics of the analysis models.

3. The predicted slope of the unloading curve for Specimen *M* is smaller (i.e., more gradual) than that obtained in the

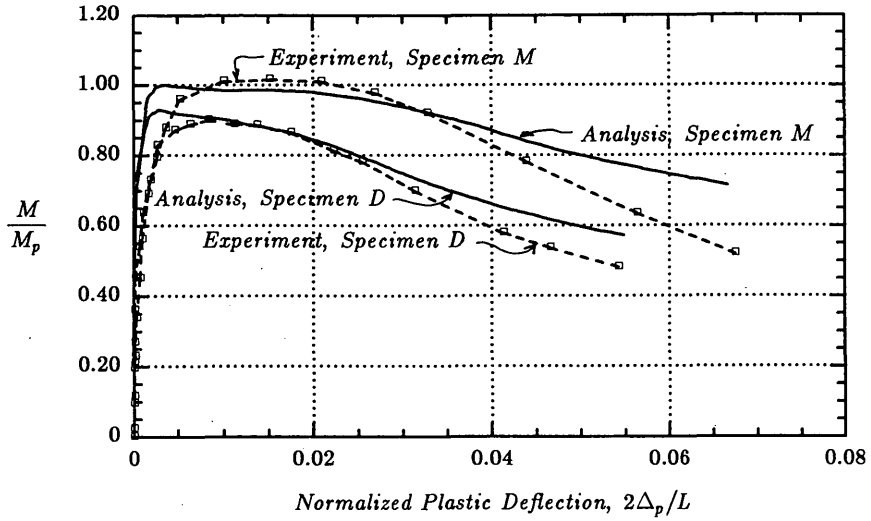

FIGURE 9 Normalized moment versus plastic deflection at midspan: Specimen *M* (*L* = 78 in.) and Specimen *D* (L = 84 in.).

physical test. Similar characteristics in the unloading region are exhibited for Specimen *D*. This may be caused by differences between the failure mode predicted by the analysis and that obtained in the experiment.

4. Similarly to the behavior exhibited in the analysis of Specimen *S*, the web initially distorts under flexural compression within the panel adjacent to midspan in both the analyses of Specimens *M* and *D* (the deformed finite element meshes are not shown for these tests). However, unlike Specimen *S*, the analyses of Specimens *M* and *D* indicate that final mode of failure involves a combined local instability of the web and compression flange in the short panel adjacent to midspan. This differs from the behavior reported for the experimental tests. Schilling reports that the failure mode of Specimens *M* and *D* was the same as that of Specimen *S* in the physical tests (*4*).

This discrepancy may be partly caused by differences between the assumed and the actual geometric imperfections and residual stresses. Analyses that have been performed with the use of different initial imperfections indicate that the detailed mode of failure can vary significantly on the basis of the assumed distribution of initial imperfections. However, on the basis of observations from the studies conducted, it appears that changes in the distribution of initial imperfections do not have a significant effect on the overall load-deflection behavior of these girders. Nevertheless, failure within the second panel from the load point was not obtained for any of the imperfections considered.

RESULTS FOR COMPOSITE GIRDER

The analysis results for the composite specimen are summarized in Figures 10–13. The following observations can be drawn from these studies:

1. The correlation of the load-deflection curves in Figure 10 is good, except that yielding is much more predominant

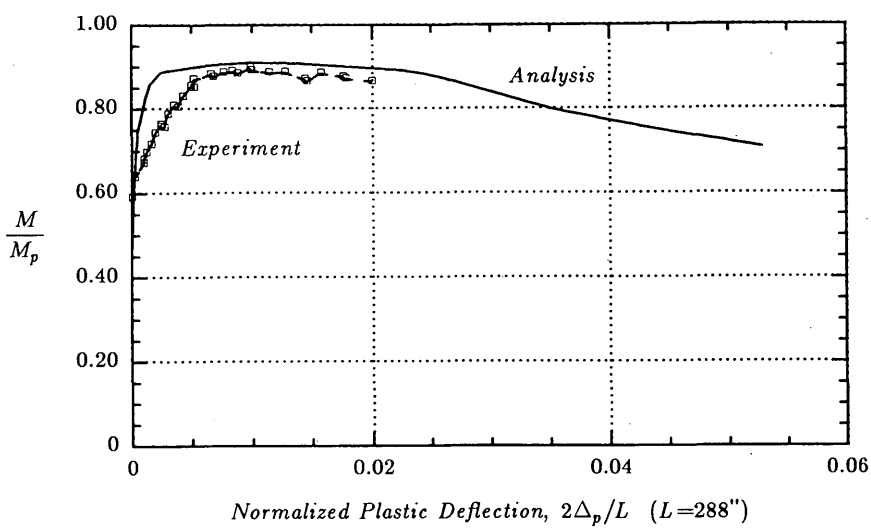

FIGURE 10 Normalized moment versus plastic deflection at midspan, composite specimen.

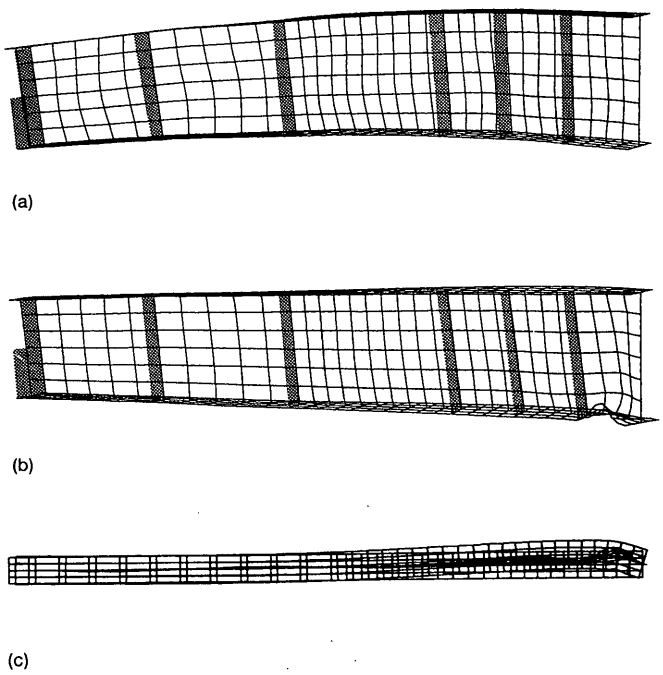

FIGURE 11 Deformed meshes, composite specimen: (a) at dead load level: M/M_p = 0.452, magnification of 20 times, (b) perspective view in post-collapse region: M/M_p = 0.885, normalized plastic deflection $2\Delta_p/L$ = 0.0250 (L = 288 in.) magnification of 2 times, and (c) top view in post-collapse region: M/M_p = 0.885, normalized plastic deflection $2\Delta_p$/L = 0.0250 (L = 288 in.), magnification of 2 times.

in the actual test in the pre-peak region of the response. In the actual test, yielding was observed at dead load levels before casting of the deck, and significant additional loading was introduced into the steel section by shrinkage of the concrete before application of the simulated live load.

2. Although the composite specimen has similar proportions to Specimen D, the moment-rotation curves for this specimen, both from the analysis and from the experiment, appear to exhibit slightly greater rotation capacity than the curves for Specimen D. Additional studies reported by White and Dutta (*10*) indicate that this difference in the behavior may be partly the result of the mode of construction. The girder, when analyzed for shored construction, exhibits moment-rotation characteristics closer to those of Specimen D.

3. The deformed shape of the girder at the full application of dead load, magnified by a factor of 20 is shown in Figure 11(a). This figure illustrates that the web of the girder is essentially buckled at very low load levels. However, the buckling distortions are small and are noticeable only when highly magnified, such as in the figure.

4. The mode of failure in the analysis of the composite girder involves initially a "bend buckling" of the web panel adjacent to midspan, constrained by the compression flange and transverse stiffeners. However, local buckling in the compression flange is soon precipitated by these web distortions. Finally, the compression flange appears to fail in a mode involving large lateral movement within the unbraced length adjacent to the load point. The combination of all these modes of failure is illustrated by the plots in Figures 11b and 11c, which are taken at an intermediate point along the unloading curve of Figure 10. The primary failure in the experiment occurred in the second panel from midspan. This may be partly caused by the additional restraint provided to the compression flange by a bearing plate at the load point in the actual test. The bearing plate was not considered in the analysis.

5. Unfortunately, the experimental test was halted prematurely because of the failure of the braces at the one-quarter span points. This prompted a study of the brace forces predicted by the analysis at these points. In Figure 12 these forces are plotted as a percentage of the compression flange yield load versus the normalized moment at the midspan of the girder. It is evident that after the girder becomes plastified at midspan, the forces at the one-quarter span brace points increase rapidly. If the full plastic deformations exhibited by the curves in Figure 10 are to be developed, the analysis predicts that these braces need to resist a force of 3.7 percent of the compression flange yield load. The initial brace force

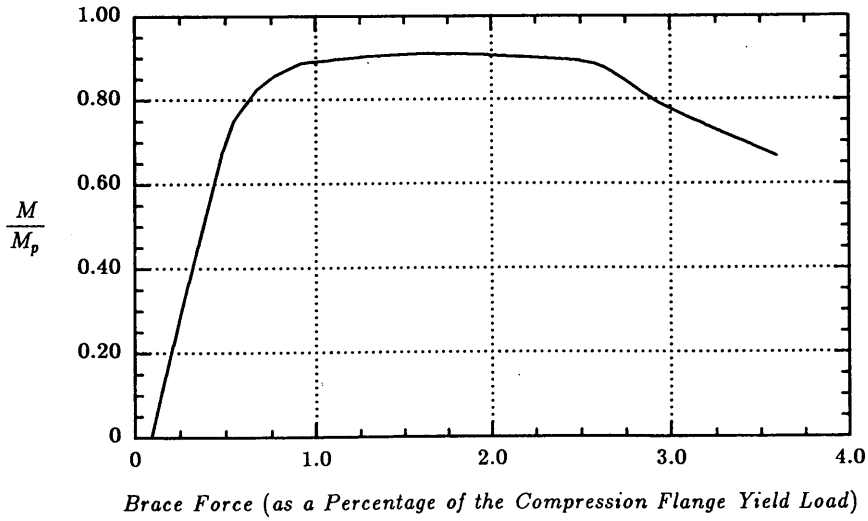

FIGURE 12 Normalized moment versus brace force at the quarter-span location—composite specimen.

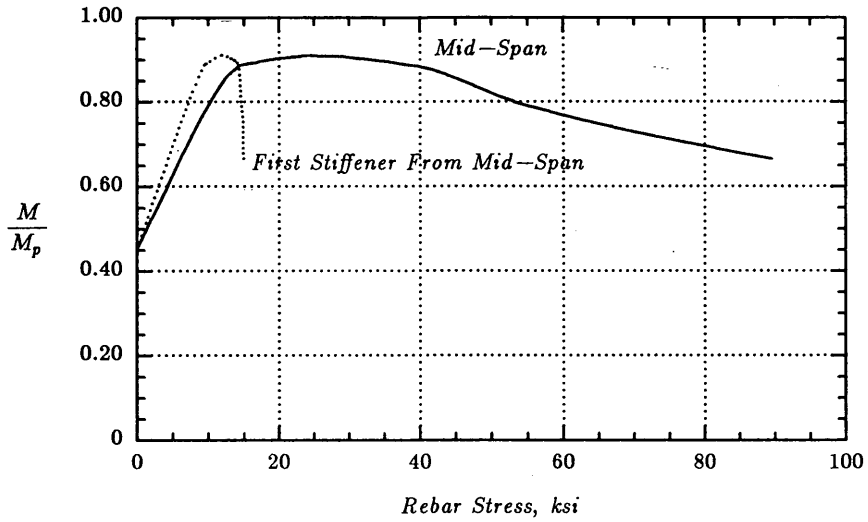

FIGURE 13 Normalized moment versus stresses in the top layer of reinforcing steel—composite specimen.

at zero applied load in Figure 12 is because of the equilibration of the specified residual stresses in the first increment of the analysis.

6. The stresses in the reinforcing steel at the simulated interior-pier location are of significant interest. An important ALFD criterion aimed at control of concrete cracking is that the stress in the rebars at overload must be below the yield stress. The rebar stresses are below the yield stress of the reinforcing steel (72.5 ksi) for practically the full range of loading conducted in the analysis (see Figure 13). The analysis as well as the experiment indicate that, as the bottom portion of the girder web and the compression flange lose their stability, the neutral axis at midspan moves above the theoretical depth associated with the plastic moment M_p (*10*).

CONCLUSIONS

It can be concluded that the finite element studies provide a reasonable estimate of the behavior exhibited in the experimental tests. Also, the analysis solutions are helpful to gain an improved understanding of the structural performance. The numerical studies and experimental tests indicate that noncompact continuous span bridge girders of the types considered exhibit a significant and reliable capacity for inelastic rotation over interior supports.

ACKNOWLEDGMENTS

This project was sponsored by the American Iron and Steel Institute, and was conducted under the guidance of the Project 51 Task Force. The advice and assistance of the AISI staff and members on the Project 51 Task Force are gratefully acknowledged.

REFERENCES

1. *Guide Specifications for Alternate Load Factor Design Procedures for Steel Beam Bridges Using Braced Compact Sections*. American Association of State Highway and Transportation Officials, Washington, D.C., 1986.
2. C. G. Schilling. *A Unified Autostress Method*. Report on Project 51, American Iron and Steel Institute, Washington, D.C., Nov. 1989.
3. C. G. Schilling. Moment-Rotation Tests of Steel Bridge Girders. *Journal of Structural Engineering*, American Society of Civil Engineers, New York, N.Y., Vol. 114, No. 1, 1988, pp. 134–149.
4. C. G. Schilling and S. S. Morcos. *Moment-Rotation Tests of Steel Girders with Ultracompact Flanges*. Report on Project 188, American Iron and Steel Institute, Washington, D.C., July 1988.
5. T. C. Tansil. *Behavior of a Composite Plate Girder in Negative Bending*. M.S. thesis. University of Texas, Austin, Tex., Dec. 1991.
6. A. Vasseghi and K. H. Frank. *Static Shear and Bending Strength of Composite Plate Girders*. PMFSEL Report 87-4, Department of Civil Engineering, University of Texas, Austin, Tex., June 1987.
7. *Specification for the Design, Fabrication, and Erection of Structural Steel for Buildings*, American Institute of Steel Construction, Chicago, Ill., 1978.
8. *Standard Specifications for Highway Bridges*, 14th ed., and Interim Specifications through 1991. American Association of State Highway and Transportation Officials, Washington, D.C., 1989.
9. C. G. Schilling. *Exploratory Autostress Girder Designs*. Report on Project 188, American Iron and Steel Institute, Washington, D.C., July 1986.
10. D. W. White and A. Dutta. *Numerical Studies of the Inelastic Moment-Rotation Behavior of Noncompact Bridge Girders*. Structural Engineering Report CE-STR-92-1, School of Civil Engineering, Purdue University, W. Lafayette, Ind., Nov. 1991.
11. N. G. Cofie and H. Krawinkler. Uniaxial Cyclic Stress-Strain Behavior of Structural Steel. *Journal of Engineering Mechanics*, American Society of Civil Engineers, New York, N.Y., Vol. 111, No. 9, 1985, pp. 1105–1120.
12. *Ultimate Limit State Calculation of Sway Frames with Rigid Joints*. European Convention for Constructional Steelwork, Publication 33, Technical Working Group 8.2, Systems, Nov. 1983.
13. P. S. Carskaddan. *Autostress Design of Highway Bridges, Phase 3: Interior-Support-Model Test*. Project 188, American Iron and Steel Institute, Washington, D.C., Feb. 1980.